

Article

Modeling of the Temperature Profiles and Thermoelectric Effects in Phase Change Memory Cells

Changcheng Ma, Jing He, Jingjing Lu, Jie Zhu and Zuoqi Hu *

School of Optical and Electronic Information, Huazhong University of Science and Technology, Wuhan 430070, China; D201477521@hust.edu.cn (C.M.); D201577534@hust.edu.cn (J.H.); lu_2014@hust.edu.cn (J.L.); m201672049@hust.edu.cn (J.Z.)

* Correspondence: hu_zuoqi@hust.edu.cn

Received: 31 May 2018; Accepted: 11 July 2018; Published: 27 July 2018



Featured Application: This work can be used for the optimal design of higher efficiency phase change memory (PCM) cells.

Abstract: Phase change memory (PCM) is an important element in the development and realization of new forms of brain-like computing. In this article, a three-dimensional finite element method simulation is carried out to study the temperature profiles within PCM cells for a better understanding of switching operations. On the basis of a finite difference method, the simulation consists of phase transition kinetics, electrical, thermal, percolation effect, as well as thermoelectric effects, using temperature-dependent material parameters. The Thomson effect within the phase-change material and the Peltier effect at the electrode contact are respectively considered for a detailed analysis of the impact on the temperature profiles and the programming current for switching processes. The simulation results show that switching operations are primarily implemented by the melting and quenching of the phase-change material close to the contact between the bottom electrode and phase change material, and its final phase distribution is determined by the cooling rate. With positive current polarity, thermoelectric effects improve heating efficiency and then reduce the programming current. Because of the different occurrence region, the Peltier effect significantly changes the temperature profile, which is more influential in switching operations. Additionally, the contribution of thermoelectric effects decreases with the cell size scaling because of the weakening of the Peltier effect. This paper aims at providing a more precise description of the thermoelectric phenomena taking place in switching operations for future PCM design.

Keywords: phase change memory; finite element modeling; temperature profiles; thermoelectric effects; cooling rates

1. Introduction

Recently, phase change memory (PCM) has received much attention as an attractive next generation memory technology because of its benefits, such as fast its programming speed, non-volatility, low cost, promising scalability, good endurance, and capability of performing complicated non-binary arithmetic processing and computation [1–6]. PCM cells store data by means of reversible transitions between conductive crystalline (SET) and highly resistive amorphous (RESET) states of a small active region within phase change materials (common $\text{Ge}_2\text{Sb}_2\text{Te}_5$ (GST) [7]), induced by appropriate heating via electrical pulses. RESET operation requires a short and intense electrical pulse to heat the active region above its melting temperature, and a subsequent rapid quenching solidifies the GST materials into the amorphous state allowing it insufficient time to crystallize. The reverse process, SET operation, involves recrystallization of the amorphous region formed during the RESET

operation, where a moderate amplitude longer duration pulse is used to switch the amorphous region back to a crystalline state through annealing above crystallization temperature or melting followed by slower cooling.

Given the large temperature gradients and current densities during the switching operation, thermoelectric effects have a large impact on the performance of PCM cells [8]. The thermoelectric effects are the result of the energy exchange between the charge carriers and the lattice in the presence of an electric current [9]. When the junction of different materials is heated, electrons are enabled to pass from the material in which the electrons have the lower energy into that in which their energy is higher, giving rise to an electromotive force, namely the Seebeck effect. The Peltier effect appears as heating/cooling at the junction, because the energy transported by the electrons is altered when a current passes from one material to another. The Thomson effect consists of reversible heating or cooling as charge carriers absorb or release energy along a uniform material under an electrical current due to a temperature gradient. These thermoelectric effects influence the temperature profiles within the cell through heating or cooling depending on the direction of current, and then change the final phase distribution and the corresponding resistance of the cell.

For future cell design, it is necessary to investigate these thermoelectric phenomena in detail. Owing to the short phase change timescales involved and the small length scales of actual PCM cells, quite a few numerical simulations have been executed for a systematic analysis of the PCM cell operations, however they have typically neglected the phase change process or not included the thermoelectric effects [8,10–12]. In reality, the phase-change behavior is closely related to the temperature and its history. The final phase distribution cannot be accurately captured only using the temperature profile, especially in the SET operation, which requires enough temperature and time for crystallization. A model containing phase change kinetics is essential for a comprehensive study of the thermoelectric effects during the PCM cell operations.

In this article, we employed a three-dimensional finite element simulation to study the temperature profiles within the PCM cells, which is available for arbitrarily complex cell structure. We carry out electrical, thermal, and phase change simulations for a complete description of switching operations in the PCM cells, considering the temperature dependence of material parameters. The thermoelectric effects are included by the modification of the current continuity equation and the heat conduction equations. The simulated temperature profiles are studied in detail for the analysis of thermoelectric effects in switch processes. The impact of isotropic scaling on thermoelectric effects is also addressed.

2. Model and Materials

2.1. Model

The geometry of the simulated mushroom PCM cell is shown in Figure 1. The mushroom cells are more relevant for the PCM industry because of the higher density storage and greater susceptibility to thermoelectric heating due to asymmetric geometries. The cell consists of a W (tungsten) top electrode contact, a TiN (titanium nitride) shared top electrode, a GST phase change layer, a TiN narrow bottom electrode (BE), and a W plug surrounded by the thermal and electrical insulation (SiO_2) with dimensions provided in the Figure 1. The TiN electrode, which has a lower thermal conductivity, acts to confine the energy in the GST layer. An ideal square-wave electrical pulse is biased on the W top electrode contact while the W bottom electrode contact is grounded, which is referred to as the positive bias pulse. A small pulse is applied to calculate the electrical resistance of the cell.

In this study, we adopt the finite difference method, in which a model space is discretized into three-dimensional Cartesian grids according to the complex geometry of PCM cells with arbitrary cell configuration. The model includes four individual sub-models: electrical, thermal, phase change, and percolation, for a complete description of switching operations in the PCM cells.

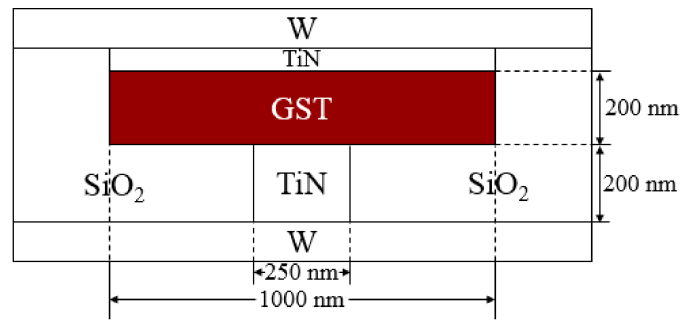


Figure 1. Cross-sectional view of the simulated mushroom phase change memory (PCM) cell.

The spatial electrical potential distribution in the cells are modeled by iteratively solving the current continuity equation for each mesh element, and considering particularly the additional current generated due to the Seebeck effect. The calculated electrical current in each mesh element induces local heating as a heat source known as Joule heat. Subsequent heat diffusion changes the temperature distribution, which is calculated by solving the heat conduction equation. Because of the significant contribution compared with Joule heating, thermoelectric heating, consisting of Thomson heat within the GST layer and Peltier heat at the GST–BE interface, should also be considered.

The current continuity (1) and heat conduction (2) equations are modified to include the thermoelectric effects and are given by

$$\nabla \cdot J = -\nabla \cdot (\sigma(\nabla V + S\nabla T)) = 0, \tag{1}$$

$$dC_p \frac{dT}{dt} - \nabla \cdot (\kappa \nabla T) = \frac{J \cdot J}{\sigma} - TJ \cdot \Delta S - TJ \cdot \frac{dS}{dT} \nabla T, \tag{2}$$

where J is the current density, σ is the electrical conductivity, V is the electric potential, S is Seebeck coefficient, T is the temperature, d is the mass density, and C_p is the heat capacity. The thermoelectric contributions are included as thermally driven diffusion current ($-\sigma \cdot S \nabla T$) in Equation (1) and thermoelectric heat transport ($-TJ \cdot \nabla S$, Peltier heating and $-TJ \cdot (dS/dT) \nabla T$, Thomson heating) in Equation (2) [10].

The classical theory of nucleation is applied in the phase change model to study switching characteristics according to the calculated temperature distribution [11]. Here, we consider homogenous and heterogeneous nucleation in the bulk material and at interfaces to simulate the crystallization process. The temperature dependent nucleation rate, the growth velocity of the nuclei and the probabilities of crystallization via nucleation or growth are also included. The overall physical property changes of the phase change material, referred to as the percolation effect, are calculated by Bruggeman effective medium approximation [13].

2.2. Materials

The parameters used in the model at zero electric field and room temperature (300 K) are shown in Table 1 [11].

Table 1. Numerical values for electrical conductivity ρ , thermal conductivity κ , and specific heat C of SiO_2 , TiN, and W.

	ρ_{elec} (Ω m)	κ (W/m K)	C (J/Kg K)
SiO_2	10^{14}	1.3	1050
TiN	10^{-6}	14	784
W	5.4×10^{-8}	175	132

Temperature dependent electrical resistivity of crystalline (fcc) and amorphous GST close to room temperature is extrapolated up to T_{melt} (Figure 2a) to model the metastable $\rho(T)$ functions [14]. A constant value of $\rho_{liquid} = 5 \mu\Omega \cdot m$ is used for liquid GST [15].

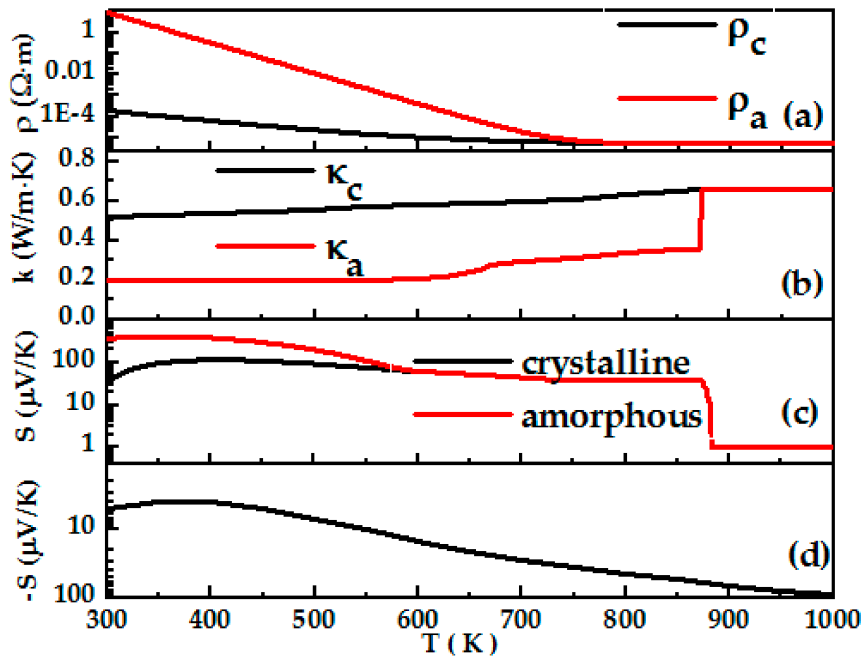


Figure 2. (a) Electrical conductivity of crystalline and amorphous $\text{Ge}_2\text{Sb}_2\text{Te}_5$ (GST); (b) thermal conductivity of GST with phonon and electronic contributions shown; (c) heat capacity for GST with a plateau at melting to include latent heat of fusion; (d) Seebeck coefficients for GST in amorphous and crystalline phases; (e) negative Seebeck coefficient of TiN.

The thermal conductivity (κ) of solid GST [Figure 2b] is approximately the sum of a phonon contribution (κ_{ph}), which is assumed to be independent on the temperature [16], and an electronic contribution (κ_{el}), which is calculated using the Wiedemann–Franz law [17]. Thermal conductivity of liquid GST is assumed to be dominated by κ_{el} .

Seebeck coefficients of GST (Figure 2c) are measured up to 740 K, and modeled to be constant between 800 K and 873 K, and assumed to have a constant value of $1 \mu\text{V}/\text{K}$ in the liquid phase [18]. Seebeck coefficients for TiN (Figure 2d) are measured in the 300–800 K range and extrapolated to 1000 K [8].

The specific heat (C_p) of the GST layer is assumed as a constant value of $202 \text{ J}/(\text{kg} \cdot \text{K})$, which is independent on the temperature and the phase state. The latent heat of the amorphous-to-crystalline transformation ΔH_v is taken from Ref. [19]. This work has some limit due to the fact that the thermal boundary resistances (TBR) is not included in the focus on thermoelectric effects, and the effect of TBR requires further study.

3. Results and Discussion

3.1. RESET Operation

The simulated temperature distribution within the mushroom PCM cell at the time of maximum temperature occurrence, that is the end of the RESET pulse, is plotted in Figure 3a, where thermoelectric effects are not considered. Although our model is a three-dimensional finite element simulation, all the results are given in two-dimensions to be able to compare the variation of temperature profiles and phase distributions with and without thermoelectric effects more plainly and clearly. A 2.6 mA, 50 ns input pulse is applied to heat the GST material adjacent to the GST–BE interface above

its melting temperature, and it subsequently cools into the amorphous phase. The crystallization fraction (f) inside the GST layer is shown in Figure 3b. The GST–BE interface is completely covered by the amorphous GST plug, forming a high-resistance path on readout between the top and bottom electrodes. The corresponding cell resistance increases two orders of magnitude as compared to the original value, and then the RESET operation is accomplished.

From the above, the temperature distribution governs the formation of the amorphous region and the resulting cell resistance. Hence, through strongly altering the temperature distribution within the PCM cells, thermoelectric effects can influence the current for successful RESET. Figure 4 shows the temperature profiles within the PCM cells at the end of the pulse with the same current pulses (2.5 mA, 50 ns) for both positive and negative polarities. With the positive polarity current, both the Peltier effect and the Thomson effect can improve the heating efficiency and then expand the volume of the molten region, which is beneficial to form enough amorphous zone for the RESET operation with lower pulse amplitude. Additionally, the cell requires more current because of the cooling induced by the thermoelectric effects under negative current polarity.

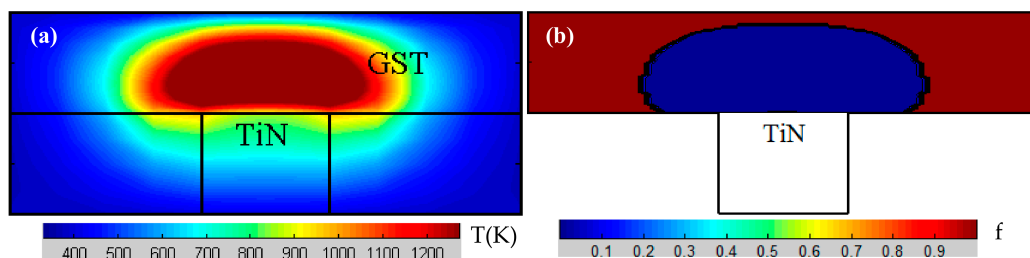


Figure 3. (a) Temperature distribution within the simulated cell at the end of the pulse; (b) corresponding phase distribution in the GST layer, with blue and red regions representing the amorphous and crystalline phase, respectively.

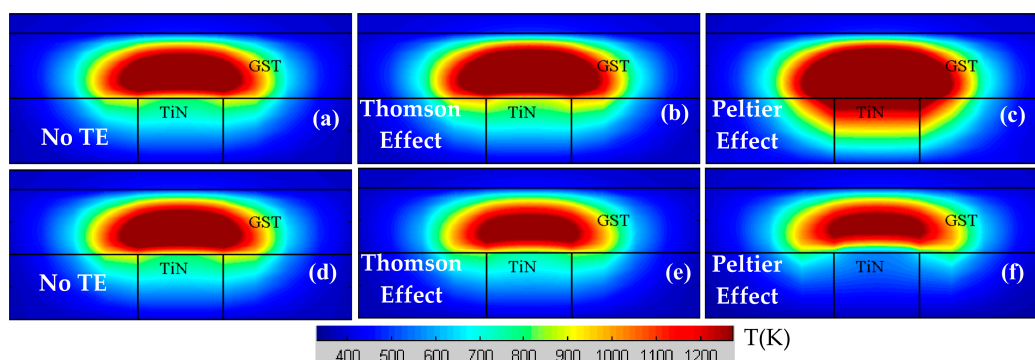


Figure 4. Temperature profiles within the cells at the end of the pulse (2.5 mA, 50 ns) for positive (a–c) and negative (d–f) polarities, including no thermoelectric effects (a,d), only Thomson (b,e), and only Peltier heating (c,f).

Because of the different occurrence region, these thermoelectric effects have different influences on the temperature profiles. The Thomson effect mainly occurs in the GST materials, and slightly raises the temperature reached in the GST layer, shown in Figure 4b, similar to the results of the pulse amplitude increasing. The Peltier effect in the cell with the 250 nm width bottom electrode, simulated in this paper, results in a larger change in the thermal profiles compared with the Thomson effect (Figure 4c), because of the greater energy released in the active region and, more importantly, a more critical location at the GST–BE interface. Therefore, the Peltier effect can cause the position of the hot spot to shift towards the GST–BE interface, heat the GST material near the interface more easily, and then, vastly influence the result of the RESET operation. On the contrary, the Peltier effect hinders the RESET operation more seriously with the negative polarity, as plotted in Figure 4f.

The cell resistance as a function the RESET current is plotted in Figure 5. The current polarity has no impact on the RESET current (solid squares) when neglecting thermoelectric effects. In addition, the Peltier effect can force the programming current down to 2.3 mA in the positive bias and up to 2.95 mA in the reverse bias (solid circles), respectively. The RESET programming current polarity in the simulation (2.3–2.95 mA) is close to that in the literature data (2.3–3.2 mA, hollow circles) [20], which confirms our simulation. Thomson heating in the mushroom cell is simulated as a contribution to 5% of the programming current reduction.

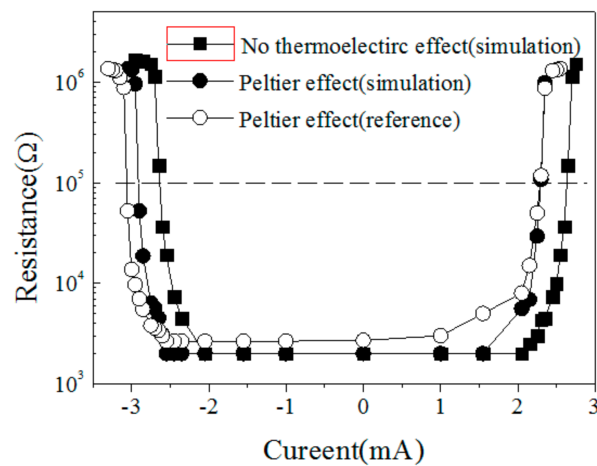


Figure 5. Cell resistance as a function the RESET current for a fixed pulse width of 100 ns with and without Peltier effect.

The impact of isotropic scaling on thermoelectric effects is also addressed. The cell size-scaling can result in the reduction of the RESET current and change the corresponding thermal profiles, so the impact of thermoelectric effects on the RESET operation is influenced, shown in Figure 6. The programming current reduction, compared with the results neglecting thermoelectric effects, represents the contributions of Thomson and Peltier heating to the RESET operation. The contribution of the Thomson effect basically keeps constant regardless of the size scaling (solid circles). However, the influence of the Peltier effect on programming current gradually weakens, resulting in the decrease of current reductions induced by thermoelectric effects. Given the cell size aggressive scaling trends, the effect of scaling on the thermoelectric effects requires further investigation for the design of PCM cells.

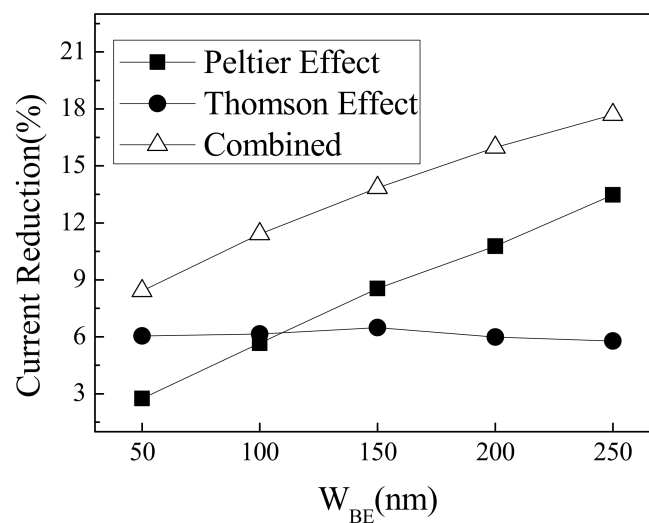


Figure 6. Impact of thermoelectric effects on the programming current for the RESET operation with the bottom electrode width (W_{BE}) scaling from 250 nm to 50 nm, assuming isotropic downscaling.

3.2. SET Operation

Reversible switching in the PCM cell is achieved by recrystallization of the amorphous GST material in the phase change layer. In common, the PCM cell in the RESET state, in which a portion of GST material near the GST–BE interface is in the amorphous state after a RESET operation, is utilized for the SET operation. Simulations for the PCM cell with the phase distributions in Figure 3b is biased on a 1.9 mA, 150 ns positive pulse for the SET operation. At the end of pulse, the temperature of the central part of the initially amorphous region exceeds the melting temperature of the GST material, and the cell temperature decreases from this inner region in an outwards direction, as plotted in Figure 7a. When the current pulse is removed, the whole cell begins to cool down. The central molten region cools into an amorphous state due to the large cooling rate comparable to that of the RESET operation, and the GST material close to the GST–BE interface experiences crystallization, as shown in Figure 7b. The crystalline high-conductive current path between the top and bottom electrodes determines the low-resistive state of the cell, which means the implement of SET operation.

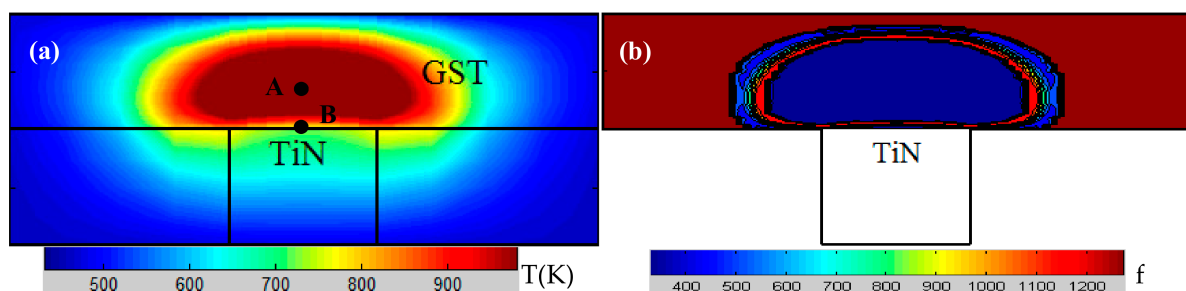


Figure 7. (a) Temperature profiles of the cells at the end of the current pulse (1.9 mA, 150 ns), point “A” represents the position of the hot spot while point “B” is located at the center of the GST–BE interface; (b) corresponding phase distribution within the GST layer. Blue and red regions represent the amorphous and crystalline phase, respectively.

Since the phase change dynamics in the case of the SET operation is rather complex as compared to the RESET operation, the temperature history within the PCM cell was simulated for further analysis. For example, in Figure 8a we compare the temporal evolution of the temperature at the position of the hot spot (A) and the center of the GST–BE interface (B), marked in Figure 7a. The temperature of whole cell increases rapidly at first and reaches the maximum at the end of the SET pulse. The heating/cooling rate is further calculated by the derivative of dT/dt from the temperature curve, as shown in Figure 8b. The heating rates of the two positions are both maximum at the beginning of the pulse, and drop quickly up to become flat, which always stay above 0.8 K/ns. The following cooling rate rapidly increases to its maximum value at the first several nanoseconds (3 ns), and subsequently drops down.

Since the simulated crystallization kinetics in the PCM cell is quite different from that based on the isothermal annealing process, the heating rate in the SET process should be considered, and its effects on crystallization start temperature (T_c) were also studied by other groups [21,22]. On the basis of these results, Choi et al. [21] gave an empirical relation between T_c ($^{\circ}\text{C}$) and heating rate (α , $^{\circ}\text{C}/\text{min}$) as below

$$T_c(\alpha) = -84.32 + 52.60 \cdot \ln(\alpha + 79.98). \quad (3)$$

According to the heating rate above, the calculated crystallization start temperature exceeds 1600 K, far beyond the temperature reached in the GST layer, shown in Figure 8a. It indicates that crystallization is almost prohibited during the heating process because of the relatively high T_c caused by the excessive heating rate. That is contradictory to our simulation results in Figure 7b, where crystallization occurs at the GST material adjacent to the GST–BE interface. Therefore, we believe that crystallization most likely occurs during the cooling process.

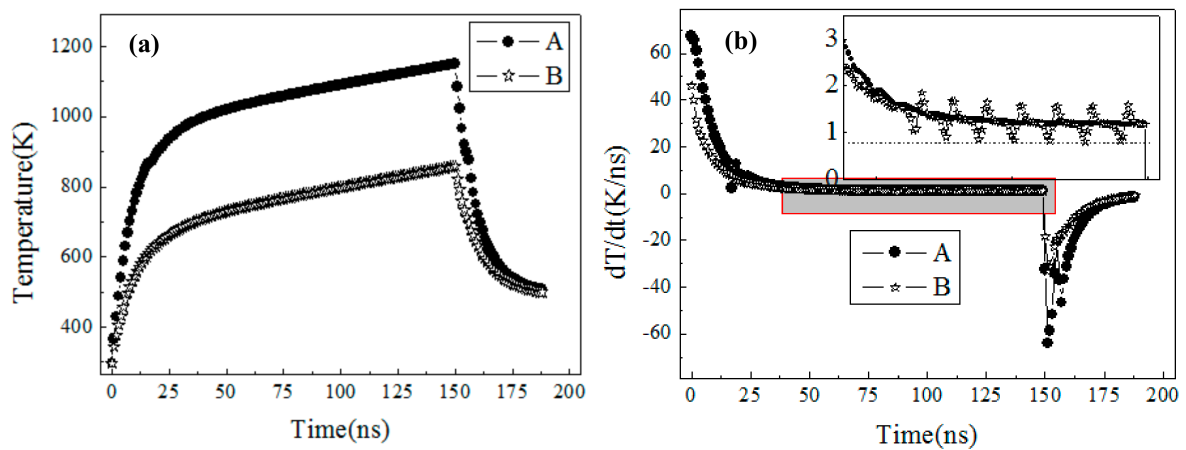


Figure 8. (a) Variations of the temperature and (b) heating/cooling rate at two different positions in the GST layer. A at the position of the hot spot in the GST layer and B at the center of the GST–BE interface which marked in Figure 7a, respectively.

The cooling process in the GST layer was studied in detail, and the temperature variation between the A and B points is plotted in Figure 9. Because of the asymmetry of the cell structure, the central part can reach higher temperature, and then cools down more rapidly. It is well known that crystallization temperature and crystallization time determine the formation of small crystalline nuclei of critical size and their subsequent growth, respectively. During the cooling stage, the crystallization proceeds as the temperature drops from melting temperature (T_m) to crystallization temperature (T_c), shown as the dotted line in Figure 9. Compared with the final phase distribution in Figure 7b, only the GST material at the center of the GST–BE interface has a long crystallization time, leading to complete crystallization together with grain growth. For the annular-like temperature distribution in the PCM cell, there is an annular crystalline region formed in the PCM cell. The inner part has insufficient time for grain growth, and the GST material in the outer part does not crystallize due to insufficient heating. Hence, the phase change dynamics in the case of the SET operation are more rigorous to the temperature than that of the RESET operation; the GST material near the GST–BE interface requires a high enough temperature and a proper cooling rate for complete crystallization.

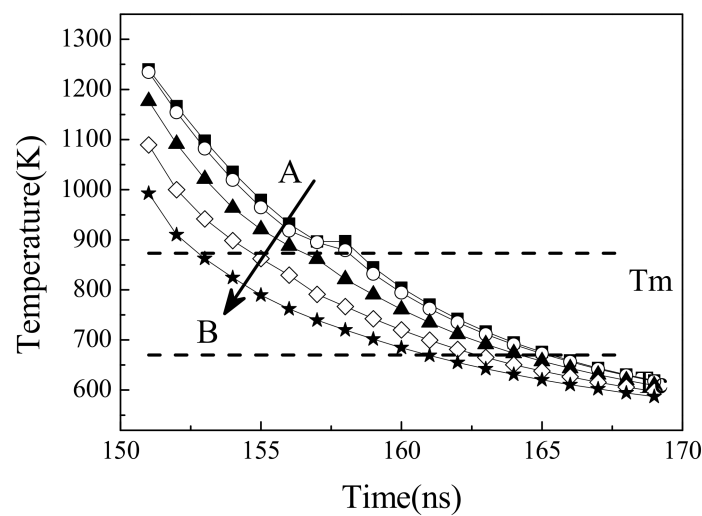


Figure 9. Temperature variation between the A and B points in the cooling stage, the arrow indicates the five points from A to B in Figure 7a.

The impact of thermoelectric effects on the SET operation is now discussed in this paper. Figure 10a shows the temperature profiles of the cells at the end of the SET pulse with and without thermoelectric effects. Similarly, under the positive current polarity, the thermoelectric effects improve the heating efficiency to bring the GST materials up to a higher temperature with the same current pulse. Because of releasing thermal energy at the GST–BE interface, the Peltier effect expands the temperature distribution vertically, which results in a vertically broader high-conductive current path formation and then contacts the top and bottom electrodes more easily, as shown in Figure 10b. Therefore, the contribution of Peltier heat to the programming current reduction (17%) is larger than that of Thomson heat (11%) with the same pulse width of 150 ns.

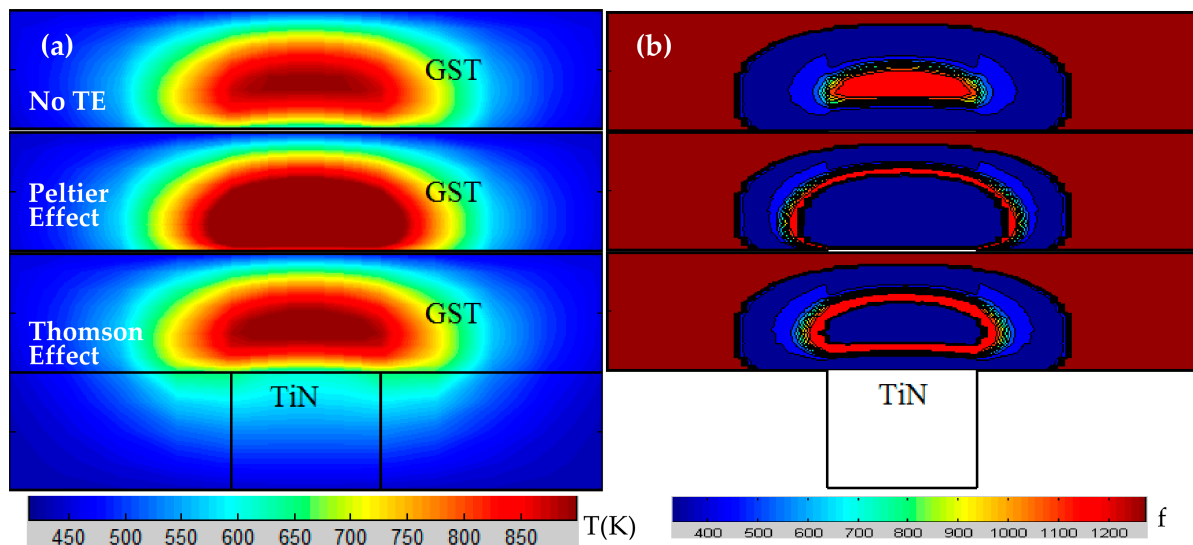


Figure 10. (a) Temperature profiles of the cells at the end of the current pulse (1.5 mA, 150 ns) with and without thermoelectric effects; (b) corresponding phase distribution within the GST layer. Blue and red regions represent the amorphous and crystalline phase, respectively.

4. Conclusions

This paper studies the temperature profiles within mushroom PCM cells, using a three-dimensional finite element simulation model. On the basis of practical application objectives, the electrical, thermal, phase change, and percolation dynamics during the switching processes were simulated in turn using the finite difference method. The simulation results show that both RESET and SET operations are implemented by the melting and quenching of the GST material close to the GST–BE interface, mainly depending on the cooling rate. A higher efficiency of PCM cells can be achieved by virtue of thermoelectric heating with positive current polarity. In terms of the simulated geometry and materials in this article, the Peltier effect is more powerful and occurs at a more critical location, while its influence on programming current gradually weakens with the cell size scaling, resulting in a decreased contribution of total thermoelectric effects. These results provide physical insights into switching operations and thermoelectric effects in PCM cells, which is necessary for effective cell engineering. The cell geometry and material properties can strongly influence the temperature profiles and the programming currents, and the thermoelectric effects are closely related to the temperature and the temperature gradients. Further researches are needed for the development of PCM cells with a higher thermal efficiency focused on the utilization of thermoelectric effects related to different geometry and materials.

Author Contributions: Conceptualization, C.M. and J.H.; Methodology, C.M.; Formal Analysis, C.M., J.L. and J.Z.; Writing–Original Draft Preparation, C.M.; Writing–Review & Editing, J.H., J.Z. and Z.H.

Funding: This research was funded by National Key Research and Development Plan.

Conflicts of Interest: The authors declare no conflict of interest.

References

1. Ciocchini, N.; Ielmini, D. Pulse-induced crystallization in phase-change memories under set and disturb conditions. *IEEE. Trans. Electron Dev.* **2015**, *62*, 847–854. [[CrossRef](#)]
2. Simpson, R.E.; Krbal, M.; Fons, P.; Kolobov, A.V.; Tominaga, J.; Uruga, T. Toward the ultimate limit of phase-change in $\text{Ge}_2\text{Sb}_2\text{Te}_5$. *Nano Lett.* **2010**, *10*, 414–419. [[CrossRef](#)] [[PubMed](#)]
3. Loke, D.; Lee, T.H.; Wang, W.J.; Shi, L.P.; Zhao, R.; Yeo, Y.C.; Elliott, S.R. Breaking the speed limits of phase-change memory. *Science* **2012**, *336*, 1566–1569. [[CrossRef](#)] [[PubMed](#)]
4. Wong, H.S.P.; Raoux, S.; Kim, S.; Liang, J.; Reifenberg, J.P.; Rajendran, B. Phase change memory. *Proc. IEEE* **2010**, *98*, 2201–2227. [[CrossRef](#)]
5. Russo, U.; Ielmini, D.; Redaelli, A.; Lacaita, A.L. Modeling of programming and read performance in phase-change memories-Part I: Cell optimization and scaling. *IEEE. Trans. Electron Dev.* **2008**, *55*, 506–514. [[CrossRef](#)]
6. Wright, C.D.; Hosseini, P.; Diosdado, J.A.V. Beyond von-Neumann computing with nanoscale phase-change memory devices. *Adv. Funct. Mater.* **2013**, *23*, 2248–2254. [[CrossRef](#)]
7. Fallica, R.; Battaglia, J.L.; Cocco, S.; Monguzzi, C.; Teren, A.; Wiemer, C.; Varesi, E.; Cecchini, R.; Gotti, A.; Fanciulli, M. Thermal and electrical characterization of materials for phase-change memory cells. *J. Chem. Eng. Data* **2009**, *54*, 1698–1701. [[CrossRef](#)]
8. Faraclas, A.; Bakan, G.; Adnane, L.; Dirisaglik, F.; Williams, N.E.; Gokirmak, A.; Silva, H. Modeling of thermoelectric effects in phase change memory cells. *IEEE. Trans. Electron Dev.* **2014**, *61*, 372–378. [[CrossRef](#)]
9. Bakan, G.; Khan, N.; Silva, H.; Gokirmak, A. High-temperature thermoelectric transport at small scales: Thermal generation, transport and recombination of minority carriers. *Sci. Rep.* **2013**, *32*, 2724. [[CrossRef](#)] [[PubMed](#)]
10. Lee, J.; Asheghi, M.; Goodson, K.E. Impact of thermoelectric phenomena on phase-change memory performance metrics and scaling. *Nanotechnology* **2012**, *23*, 205201. [[CrossRef](#)] [[PubMed](#)]
11. Kim, D.H.; Merget, F.; Först, M.; Kurz, H. Three-dimensional simulation model of switching dynamics in phase change random access memory cells. *J. Appl. Phys.* **2007**, *101*, 064512. [[CrossRef](#)]
12. Li, Z.; Jeyasingh, R.G.D.; Lee, J.; Asheghi, M.; Wong, H.S.P.; Goodson, K.E. Electrothermal modeling and design strategies for multibit phase-change memory. *IEEE. Trans. Electron Dev.* **2012**, *59*, 3561–3567. [[CrossRef](#)]
13. Bruggeman, V.D. Berechnung verschiedener physikalischer Konstanten von heterogenen Substanzen. I. Dielektrizitätskonstanten und Leitfähigkeiten der Mischkörper aus isotropen Substanzen. *Ann. Phys.* **1935**, *416*, 636–664. [[CrossRef](#)]
14. Endo, R.; Maeda, S.; Jinnai, Y.; Lan, R.; Kuwahara, M.; Kobayashi, Y.; Susa, M. Electric resistivity measurements of Sb_2Te_3 and $\text{Ge}_2\text{Sb}_2\text{Te}_5$ melts using four-terminal method. *Jpn. J. Appl. Phys.* **2010**, *49*, 065802. [[CrossRef](#)]
15. Cil, K.; Dirisaglik, F.; Adnane, L.; Wennberg, M.; King, A.; Faraclas, A.; Silva, H. Electrical Resistivity of Liquid $\text{Ge}_2\text{Sb}_2\text{Te}_5$ Based on Thin-Film and Nanoscale Device Measurements. *IEEE. Trans. Electron Dev.* **2013**, *60*, 433–437. [[CrossRef](#)]
16. Khulbe, P.K.; Wright, E.M.; Mansuripur, M. Crystallization behavior of as-deposited, melt quenched, and primed amorphous states of $\text{Ge}_2\text{Sb}_{2.3}\text{Te}_5$ films. *J. Appl. Phys.* **2000**, *88*, 3926–3933. [[CrossRef](#)]
17. Graf, M.J.; Yip, S.K.; Sauls, J.A.; Rainer, D. Electronic thermal conductivity and the Wiedemann-Franz law for unconventional superconductors. *Phys. Rev. B* **1996**, *53*, 15147. [[CrossRef](#)]
18. Yan, F.; Zhu, T.J.; Zhao, X.B.; Dong, S.R. Microstructures and thermoelectric properties of GeSbTe based layered compounds. *Appl. Phys. A* **2007**, *88*, 425–428. [[CrossRef](#)]
19. Hyot, B.; Gehanno, V.; Rolland, B.; Fargeix, A.; Vannufel, C.; Charlet, F.; Béchevet, B.; Bruneau, J.M.; Desre, P.J. Amorphization and crystallization mechanisms in GeSbTe -based phase change optical disks. *J. Magn. Soc. Jpn.* **2001**, *25*, 414–419. [[CrossRef](#)]
20. Suh, D.S.; Kim, C.; Kim, K.H.; Kang, Y.S.; Lee, T.Y.; Khang, Y.; Park, T.S.; Yoon, Y.G.; Im, J.; Ihm, J. Thermoelectric heating of $\text{Ge}_2\text{Sb}_2\text{Te}_5$ in phase change memory devices. *Appl. Phys. Lett.* **2010**, *96*, 123115. [[CrossRef](#)]

21. Choi, Y.; Jung, M.; Lee, Y.K. Effect of heating rate on the activation energy for crystallization of amorphous Ge₂Sb₂Te₅ thin film. *Electrochem. Solid State Lett.* **2009**, *12*, F17–F19. [[CrossRef](#)]
22. Friedrich, I.; Weidenhof, V.; Njoroge, W.; Franz, P.; Wuttig, M. Structural transformations of Ge₂Sb₂Te₅ films studied by electrical resistance measurements. *J. Appl. Phys.* **2000**, *87*, 4130–4134. [[CrossRef](#)]



© 2018 by the authors. Licensee MDPI, Basel, Switzerland. This article is an open access article distributed under the terms and conditions of the Creative Commons Attribution (CC BY) license (<http://creativecommons.org/licenses/by/4.0/>).